Eur. Phys. J. C 40, 229–241 (2005)
Digital Object Identifier (DOI) 10.1140/epjc/s2005-02127-y

THE EUROPEAN PHYSICAL JOURNAL C

Universality of the transverse momentum distributions in the framework of percolation of strings

J. Dias de Deus[1], E.G. Ferreiro[2,a], C. Pajares[2], R. Ugoccioni[3]

[1] CENTRA, Instituto Superior Técnico, 1049-001 Lisboa, Portugal
[2] Departamento de Física de Partículas and Instituto Galego de Física de Altas Energías, Universidade de Santiago de Compostela, 15782-Santiago de Compostela, Spain
[3] Dipartimento di Fisica Teorica and INFN-sezione di Torino, via P. Giuria 1, 10125 Torino, Italy

Received: 15 July 2004 / Revised version: 17 December 2004 /
Published online: 15 February 2005 –

Abstract. In the framework of percolation of color sources, the transverse momentum distribution in heavy ion and $p+p$ collisions at all centralities and energies are shown to follow a universal behavior. The width of the distribution depends on the fluctuations of the number of color sources per cluster. At low densities, there are only independent single color sources, no fluctuations occur and the distribution is described by a single exponential. At very high densities, only one cluster of many color sources appears and therefore there are not fluctuations either and the hardness of the distribution is suppressed. The Cronin effect in this framework is due to a maximum of the fluctuations which decreases as the density increases. We obtain a good agreement with experimental data including the low p_{T} behavior and the spectra for different particles. We show that the transverse momentum and multiplicity distributions are related to each other in a defined way. This point is satisfied by the experimental data on $p+p$ collisions at different energies.

1 Introduction

Many data have already been collected and analyzed during past few years at the Relativistic Heavy Ion Collider (RHIC) in order to obtain a complete understanding of the dense QCD matter which is created in high energy heavy ion collisions.

These data show that the inclusive high p_{T} hadron production in Au + Au central collisions is strongly suppressed [1–3] compared to the scaling with the number of binary nucleon–nucleon collisions, N_{coll}, expected on the basis of the factorization theorem for hard processes in perturbative QCD (pQCD) [4]. The suppression is larger at forward than at mid-rapidities [5]. No suppression was found in $d+$ Au collisions [6, 7] at mid-rapidity. Furthermore, the proton and antiproton yields become similar to the pion one at $p_{\mathrm{T}} \approx 1$–$2\,\mathrm{GeV}/c$ [6]. The ratio between the yields from central and peripheral Au + Au collisions is larger for protons than for pions at $p_{\mathrm{T}} \approx 2$–$5\,\mathrm{GeV}/c$ [6]. On the other hand, at low p_{T}, the yield for pions is larger than the one for kaons, and both are larger than the one for protons [8,9]. At very low p_{T}, the spectra for all species show a characteristic behavior [9].

The data also show the disappearance of back to back jet-like hadron correlations in Au + Au collisions, contrary to what is observed in $d+$ Au and $p+p$ collisions [10, 11] and a peculiar behavior of the fluctuations in transverse momentum [12,13], with a maximum at a certain centrality given by a number of participants around $N_{\mathrm{part}} \approx 150$.

All these data have given rise to a lot of discussion and different explanations, aimed to discriminate which of these effects are caused by initial state interactions and which ones are a consequence of final state interactions.

Here we are going to concentrate on the explanations based on initial state interactions. Different mechanisms of initial state interactions have been proposed, like saturation in high density QCD through the color glass condensate (CGC) [14–16] or clustering of strings [17] in the string models. Another possibility is the shadowing through pomeron interaction in the dual parton model [18]. All these mechanisms have in common the modification of a multiple scattering pattern – in the target rest frame – or gluon interaction – in a fast moving frame.

In the framework of the color glass condensate, the number of gluons in the hadron wave function can reach saturation when their momenta become smaller than a saturation scale $Q_{\mathrm{s}}(x) \sim x^{-\lambda s} A^{1/3}$. Clustering and percolation of color sources, strings or partons, can also be seen as an initial state interaction phenomenon. In the case of strings, these are formed by color fields stretched between partons of the projectile and the target, located at the ends of the strings. These partons are embedded in the wave function of the projectile and the target [19]. In this case, above a critical density, a cluster of color sources – strings – is formed through the whole collision area.

[a] e-mail: elena@fpax1.usc.es

In both approaches, if the number of partons exceeds a critical quantity, they will begin to overlap in the transverse plane, and interact with each other, which prevents further growth of parton densities. As the number of strings is mainly determined by the number of inelastic parton–parton collisions, the density of strings is not a property of the isolated projectile. Nevertheless, since the density of strings is connected with the density of partons and since the interaction and percolation of strings takes place before the formation of final secondaries – before fragmentation, we call our effect *initial*.

From this point of view, the suppression of p_{T} and the reduction of multiplicities have the same origin [20, 21], namely, the overlapping of color sources. In both approaches, the transverse momentum distributions satisfy a scaling law which is in agreement with the experimental data. In the CGC, the suppression was predicted to be stronger outside mid-rapidity and this point was later confirmed [5]. Below, we will show that this is also the case in the framework of percolation of strings.

A more quantitative comparison of the results of both approaches shows also a remarkable agreement [22]. The fact that the results of the string clustering approach, which is a soft, QCD inspired but model dependent description, coincide with the results of the CGC picture, which is a theory deduced from perturbative QCD, induce us to think about the possibility of a smooth transition between soft and hard regimes and about a *perturbative confinement* [23].

All these features, together with a correct description of the transverse momentum fluctuations and of the low p_{T} data, point out the existence of initial state interactions. On the other hand, the disappearance of back to back jet-like hadron correlations in Au + Au collisions, contrary to what happens in d+Au collisions, seems to point out a final state interaction description such as jet-quenching [24] or interactions with partons and comovers [25].

The Cronin effect is crucial in order to discriminate which kind of interaction is working [26]. In this paper we will show that this effect is a low energy one, and it is going to disappear at higher energies and/or densities. Similar results are obtained in the framework of the CGC [27].

Before starting with the description of our model, let us remember some general features concerning the clustering.

On general grounds, in the clustering approach, one has to distinguish between two density regimes, high and low. Let us give a very simple example: the problem of throwing N_{S} coins into M boxes (one can read: production of N_{S} partons or strings in the interaction area πR^2). The distribution $P(N)$ of N coins in a box (one can read: N partons or strings in a cluster) can be studied and, in particular, the inverse normalized fluctuation k,

$$k = \frac{\langle N\rangle^2}{\langle N^2\rangle - \langle N\rangle^2}, \tag{1}$$

can be analytically calculated. At small density, $\eta = \frac{N_{\mathrm{S}}}{M} << 1$, the coins are isolated and $k \to \infty$. At large density, $\eta >> 1$, the coins are equally distributed in the boxes and, again $k \to \infty$. At some intermediate value $\eta_{\min}$, there is a minimum. In the low density regime $\eta < \eta_{\min}$, k decreases as η increases, while in the high density regime $\eta > \eta_{\min}$, k increases with η.

This behavior for the fluctuations in the number of partons or strings in a cluster will be crucial in order to explain most of the data. In this paper we will explore these points in the framework of string percolation, using the strings as our basic objects.

The use of strings could be considered as very model dependent. Nevertheless, the string structure can be derived directly from QCD under certain approximations [28–30]. In fact, a string profile can be derived from the study of correlators of gluons fields, a profile which is in agreement with the results obtained independently in lattice QCD [30].

In order to apply these ideas, we will use the following ingredients: We need to know the number of strings N_{S}. Up to RHIC energies, N_{S} in the central rapidity region is approximately twice the number of collisions, N_{coll}. However N_{S} can be larger at RHIC and LHC energies. We compute N_{S} using the quark–gluon string model, equivalent to the dual parton model [31, 32]. Most of the reasonable string models [33–39] of heavy ions collisions obtained similar results for N_{S}. This fact gives us confidence in our values. Notice that sometimes, even in experimental analyses, N_{coll} is obtained from the Glauber model without attention for taking into account energy-momentum conservation. At high energy this conservation reduces N_{coll}. In our computation of N_{S} we use a Monte-Carlo code [39], based on the quark–gluon string model, which takes into account energy-momentum conservation.

In order to obtain analytical formulae which can give an insight of the physical grounds we use a soft ($\exp(-ap_{\mathrm{T}}^2)$) transverse momentum distribution [40] and a Poisson-like multiplicity distribution for the fragmentation of one string. We are aware that a string can also produce hard particles as in the Lund string model [41], and our simplification must be seen as a first approximation which clearly would fail at very high p_{T}. In spite of this, we will show how the clustering of strings gives rise to a universal behavior of both the transverse momentum distribution and the multiplicity distribution, which are related to each other through a gamma distribution that represents the cluster weight function.

By the overlapping of soft strings, the soft spectrum gets a hard-like contribution. This behavior must be seen as complementary to what happens in parton saturation in the CGC, where the clustering of gluons results in a softer spectrum. At RHIC and LHC energies, there is a large range of p_{T} where both descriptions should coincide. Of course, we do not claim to give a description for the whole p_{T} range at fixed energy. Our explanation applies from low to intermediate p_{T} range. This range increases with the energy. At very high p_{T}, a perturbative QCD description will be necessary.

The plan of this paper is as follows: first we describe our approach and we derive the transverse momentum and multiplicity distributions, in order to compare them with experimental data in the next chapter. The comparison includes $p + p$ data and predictions for LHC energies. After

that, we discuss the effect of the clustering on the disappearance of back to back jet-like hadron correlations. We will finish with some conclusions.

2 Percolation of strings, transverse momentum and multiplicity distributions

Multiparticle production is currently described in terms of color strings stretched between the partons of the projectile and the target. These strings decay into new ones by sea q–$\overline{q}$ production, and subsequently hadronize to produce the observed hadrons. The color in these strings is confined to a small area in the transverse space, πr_0^2, with $r_0 \simeq 0.2$–$0.25\,\mathrm{fm}$. This value is obtained in the vacuum correlator method and corresponds to the correlation length of the QCD vacuum. This value is in accordance with lattice results.

With increasing energy and/or atomic number of the colliding particles, the number of exchanged strings grows, and they start to overlap, forming clusters, very much like disks in the continuum two-dimensional percolation theory. At a certain critical density $\eta_c = 1.18$–1.5 (depending on the type of employed profile functions – homogeneous or Wood–Saxon) a macroscopical cluster appears, which marks the percolation phase transition. For nuclear collisions, this density corresponds to $\eta = N_S \frac{S_1}{S_A}$ where N_S is the total number of strings created in the collision, each one of an area $S_1 = \pi r_0^2$ and S_A corresponds to the nuclear overlapping area so it depends on the impact parameter b. For very central collisions $b = 0$ and $S_A = \pi R_A^2$.

The percolation theory governs the geometrical pattern of the string clustering. Its observable implications, however, require the introduction of some dynamics in order to describe the behavior of the cluster formed by several overlapping strings. We assume that a cluster of n strings behaves as a single string with an energy-momentum that corresponds to the sum of the energy-momenta of the overlapping strings [17–20], and with a higher color field, corresponding to the vectorial sum of the color charges of each individual $\vec{Q}_1$ string. The resulting color field covers the area S_n of the cluster. As $\vec{Q}_n^2 = \left(\sum_1^n \vec{Q}_1\right)^2$, respective to one another, and the individual string colors may be arbitrarily oriented, the average $\vec{Q}_{1i}\,\vec{Q}_{1j}$ is zero, so $\vec{Q}_n^2 = n\,\vec{Q}_1^2$. $\vec{Q}_n$ depends also on the area S_1 of each individual string that comes into the cluster, as well as on the total area of the cluster S_n:

$$Q_n = \sqrt{n\frac{S_n}{S_1}}\,Q_1\ . \tag{2}$$

We take S_1 constant and equal to a disc of radius r_0. S_n corresponds to the total area occupied by n discs, which of course can be different for different configurations even if the clusters have the same number of strings. One could make reasonable alternative assumptions about the interaction among the strings, as it was studied previously [20], but the comparison with the data on the dependence of the strength of the two-body [42] and three-body Bose–Einstein correlations of the multiplicities [43], clearly favors (2).

Notice that if the strings are just touching each other, $S_n = nS_1$ and $Q_n = nQ_1$, so the strings act independently to each other. On the contrary, if they fully overlap $S_n = S_1$ and $Q_n = \sqrt{n}Q_1$, then we obtain a reduction of the color charge. Knowing the color charge Q_n, one can compute the multiplicity μ_n and the mean transverse momentum squared $\langle p_T^2\rangle_n$ of the particles produced by a cluster, which are proportional to the color charge and color field [20,21], respectively

$$\mu_n = \sqrt{\frac{nS_n}{S_1}}\,\mu_1, \quad \langle p_T^2\rangle_n = \sqrt{\frac{nS_1}{S_n}}\,\langle p_T^2\rangle_1, \tag{3}$$

where μ_1 and $\langle p_T^2\rangle_1$ are the mean multiplicity and mean p_T^2 of particles produced by a single string. We observe

$$\mu_n\langle p_T^2\rangle_n = n\mu_1\langle p_T^2\rangle_1, \quad \frac{\mu_n}{\langle p_T^2\rangle}{}_n = \frac{S_n}{S_1}\frac{\mu_1}{\langle p_T^2\rangle}{}_1\ . \tag{4}$$

The first relation denotes that the product is an extensive quantity, while the second one indicates that each cluster satisfies a scaling law that is nothing but the Gauss theorem. From the Schwinger formula, one obtains $\mu_1 = S_1\langle p_T^2\rangle_1$. From the experimental data we can fix μ_1 and $\langle p_T^2\rangle_1$, obtaining $r_0 \simeq 0.2$–$0.25\,\mathrm{fm}$ in agreement with the above mentioned QCD result.

Moreover, in the limit of high density η, one obtains

$$\left\langle n\frac{S_1}{S_n}\right\rangle = \frac{\eta}{1-\exp(-\eta)} \equiv \frac{1}{F(\eta)^2}, \tag{5}$$

and the equations (3) transform into the analytical ones [20]

$$\mu = N_{\mathrm{strings}}\,F(\eta)\,\mu_1, \quad \langle p_T^2\rangle = \frac{1}{F(\eta)}\,\langle p_T^2\rangle_1, \tag{6}$$

where μ and $\langle p_T^2\rangle$ are the total multiplicity and mean transverse momentum and N_{strings} is the total number of created strings in the considered rapidity range.

In the mid-rapidity region, the number of strings N_{strings} is proportional to the number of $A+A$ collisions, $N_{\mathrm{coll}} \sim N_A^{4/3}$ [44,45], N_A being the number of wounded nucleons of one nucleus. In this case, the density of strings becomes $\eta = N_{\mathrm{strings}}\frac{S_1}{S_A} \sim N_A^{2/3}$. At high densities, one should consider the percolation limit – all the strings overlap into a single cluster that occupies the whole nuclear overlap area. In this case, from (3) one obtains

$$\mu_A = \sqrt{\frac{N_{\mathrm{strings}}\cdot S_A}{S_1}}\mu_1, \quad \text{where } S_A = \pi R_A^2 \propto N_A^{2/3}\ .$$

In other words, the multiplicity per participant becomes independent of N_A, i.e. *saturates*.

Outside mid-rapidity, N_{strings} is proportional to the number of participants N_A instead of to the number of collisions $N_A^{4/3}$. Therefore, there is an additional suppression factor $N_A^{1/3}$ compared to central rapidity. This fact

is at the origin of the larger suppression at $y = 3$ of the observed p_{T} distributions in Au + Au and d + Au collisions.

We use (3) to compute the multiplicities, using a Monte-Carlo code based on the quark-gluon string model to generate the strings [39]. Each string is produced at an identified impact parameter. From this, knowing the transverse area of each string, we identify all the clusters formed in each collisions and subsequently compute for each of them its multiplicity in units of μ_1. The value of μ_1 was fixed by the comparison of our results with WA98 data for Pb + Pb central collisions. Our results are in agreement with SPS and RHIC multiplicity data [21].

Using the first of the equations (6) we obtain very similar results [45]. We observe a weak dependence on N_A of the rapidity density per participant at high centrality, i.e. saturation. On the other hand, in the fragmentation region, we expect the particle density per participant nucleon to be equal or even less than the nucleon–nucleon rapidity density [45]. Both features, saturation and fragmentation scaling, are in agreement with experimental data.

Until now we have presented our results concerning mean values – mean multiplicity and mean p_{T}. In order to get distributions, we will develop the following strategy: we will introduce the multiplicity and the transverse momentum distribution for the fragmentation of one string. We will weight them with the cluster function, and then we will introduce the effect of the overlapping through $F(\eta)$. We will check that we obtain the relation (6) for the mean values.

The multiplicity distribution in heavy ion collisions can be expressed [46] as a superposition of Poisson distributions with different mean multiplicities,

$$P(n) = \int \mathrm{d}N \; W(N) \; P(N, n). \tag{7}$$

The Poisson distribution $P(N, n) = \frac{\mathrm{e}^{-N} N^n}{n!}$, $N = \langle n \rangle$, represents the cluster fragmentation, while the weight factor $W(N)$ reflects the mean multiplicity distribution of the clusters, related to the cluster size distribution and to the number of strings per cluster. This quantity has contributions due to both the nuclear structure and the parton distribution inside the nucleon.

Concerning the transverse momentum distribution, one needs the distribution $f(x, p_{\mathrm{T}})$ for each string or cluster, and the mean squared transverse momentum distribution of the clusters, $W(x)$, which is also related to the cluster size distribution through the cluster tension. For $f(x, p_{\mathrm{T}})$ we assume the Schwinger formula, $f(x, p_{\mathrm{T}}) = \exp(-p_{\mathrm{T}}^2 x)$, used also for the fragmentation of a Lund string. In this formula x is related to the string tension, or equivalently to the mean transverse mass of the string. Assuming that a cluster behaves similarly to a single string but with different string tension, that depends on the number of strings that come into the cluster, we can write for the total p_{T} distribution

$$f(p_t) = \int W(x) \; f(x, p_{\mathrm{T}}) \; . \tag{8}$$

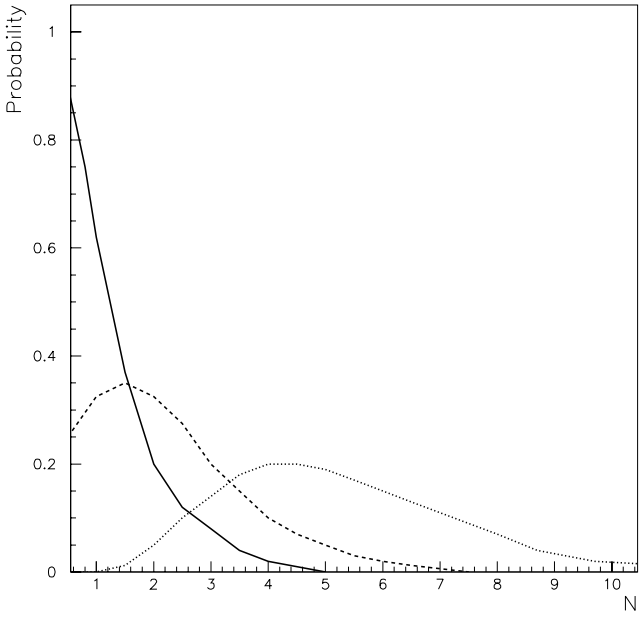

Fig. 1. Schematic representation of the number of clusters as a function of the number of strings of each cluster at three different centralities (the continuous line corresponds to the most peripheral one and the pointed line to the most central one)

The weight function $W(x)$ obeys the gamma distribution

$$W(x) = \frac{\gamma}{\Gamma(k)} (\gamma x)^{k-1} \; \exp(-\gamma x) \; . \tag{9}$$

The reason to choose a gamma distribution is the following: in peripheral heavy ion collisions, the density of strings is small and therefore there is no overlapping. The cluster size distribution in this case is peaked at low values. As the centrality increases, the density of strings also increases, so there is more and more overlapping among the strings. The cluster size distribution is strongly modified, according to the picture shown in Fig. 1, where we have plotted three cluster distributions that correspond to three increasing centralities of the collision. Each curve in Fig. 1 can be compared to a gamma distribution, with different k values. Moreover, the increase of centrality can be seen as a transformation of the cluster size distribution of the type

$$P(N) \longrightarrow \frac{NP(N)}{\langle N \rangle} \longrightarrow \ldots \longrightarrow \frac{N^k P(N)}{\langle N^k \rangle} \longrightarrow \ldots \tag{10}$$

This kind of transformations were studied long ago by Jona-Lasinio in connection to the renormalization group in probabilistic theory [47]. Actually, an increase of the centrality implies a transformation from clusters with very few strings to another set of cluster with a higher number of strings, as can be seen in Fig. 1, and a renormalization of the main variables of the clusters, i.e. mean transverse momentum and mean multiplicity, induced by the higher color of the new clusters. These transformations have been used to study the probability distribution associated to rare events [48, 49].

Introducing (9) into (7) and (8) we obtain

$$\frac{\Gamma(n+k)}{\Gamma(n+1)\Gamma(k)}\frac{\gamma'^k}{(1+\gamma')^{n+k}} = \int_0^\infty \mathrm{d}N \frac{\mathrm{e}^{-N}N^n}{n!}\frac{\gamma'}{\Gamma(k)}(\gamma' N)^{k-1}\exp\left(-\gamma' N\right) \tag{11}$$

and

$$\frac{1}{\left(1+\frac{p_\mathrm{T}^2}{\gamma}\right)^k} = \int_0^\infty \mathrm{d}x \exp\left(-p_\mathrm{T}^2 x\right)\frac{\gamma}{\Gamma(k)}(\gamma x)^{k-1}\exp\left(-\gamma x\right) . \tag{12}$$

The distribution obtained in (11) is the well known negative binomial distribution, whose mean value and dispersion verify

$$\langle n\rangle = \langle N\rangle = \frac{k}{\gamma'} , \quad \frac{\langle N^2\rangle - \langle N\rangle^2}{\langle N\rangle^2} = \frac{1}{k} ,$$
$$\frac{\langle n^2\rangle - \langle n\rangle^2}{\langle n\rangle^2} = \frac{1}{k} + \frac{1}{\langle n\rangle} . \tag{13}$$

In the distribution (12) the corresponding values are

$$\langle x\rangle = \frac{k}{\gamma} , \quad \frac{\langle x^2\rangle - \langle x\rangle^2}{\langle x\rangle^2} = \frac{1}{k} . \tag{14}$$

The parameters γ and γ' are different, since $\langle N\rangle \neq \langle x\rangle$, while k is the same in both equations.

Equations (11) and (12) can be seen as a superposition of chaotic sources – clusters – where $\frac{1}{k}$ fixes the transverse momentum fluctuations. At small density, $\eta << 1$, the strings are isolated and $k \to \infty$. When the density increases, there will be some overlapping of strings forming clusters, increasing the denominator of (1) and therefore decreasing k. The minimum of k will be reached when the fluctuations in the number of strings per cluster reach its maximum. Above this point, increasing η, these fluctuations decrease and k increases.

The distribution $W(x)$ satisfies the Koba–Nielsen–Olsen scaling, i. e. $\langle x\rangle W(x)$ depends only on $\frac{x}{\langle x\rangle}$[1]. This property [50] stems from the type of the transformations (10).

In order to take into account the effect of overlapping of strings on the multiplicity and the mean transverse momentum, we need to included our factor $F(\eta)$ in the corresponding fragmentation functions, so the Poisson distribution transforms into $P(N,n) = \frac{\mathrm{e}^{-NF(\eta)}(NF(\eta))^n}{n!}$ and the Schwinger formula transforms into $f(x, m_\mathrm{T}) = \exp(-m_\mathrm{T}^2 x F(\eta))$. Indeed, what is happening is that the invariance of the weight function under the transformation $x \to \lambda x$ and $\gamma \to \gamma/\lambda$ (or equivalently $N \to \lambda N$ and $\gamma' \to \gamma'/\lambda$), where $\lambda = F(\eta)$, leads to the changes $\langle p_\mathrm{T}^2\rangle \to \langle p_\mathrm{T}^2\rangle/\lambda$ and $\langle n\rangle \to \lambda\langle n\rangle$ in the transverse mass and multiplicity distributions respectively.

[1] However, it can depend on the energy through k.

The multiplicity distribution becomes then the universal function

$$\frac{\Gamma(n+k)}{\Gamma(n+1)\Gamma(k)}\frac{(\gamma'/F(\eta))^k}{(1+(\gamma'/F(\eta)))^{n+k}} = \frac{\Gamma(n+k)}{\Gamma(n+1)\Gamma(k)}\frac{(k/(\langle n\rangle_1 F(\eta)))^k}{(1+((k/(\langle n\rangle_1 F(\eta))))^{n+k}} \tag{15}$$

and the transverse momentum distribution behaves as

$$f(p_\mathrm{T}, y) = \frac{\mathrm{d}N}{\mathrm{d}y}\frac{k-1}{\gamma/F(\eta)}\frac{1}{\left(1+\frac{p_\mathrm{T}^2}{\gamma/F(\eta)}\right)^k} = \frac{\mathrm{d}N}{\mathrm{d}y}\frac{k-1}{k\langle p_\mathrm{T}^2\rangle_1}F(\eta)\frac{1}{\left(1+\frac{F(\eta)}{k}\frac{p_\mathrm{T}^2}{\langle p_\mathrm{T}^2\rangle_1}\right)^k} . \tag{16}$$

The above equation has been normalized to

$$f(p_\mathrm{T}, y) = \frac{\mathrm{d}N}{\mathrm{d}p_\mathrm{T}^2\mathrm{d}y} . \tag{17}$$

In the new distributions, $\langle p_\mathrm{T}^2\rangle = \langle p_\mathrm{T}^2\rangle_\mathrm{old}/F(\eta)$ and $\langle n\rangle = F(\eta)\langle n\rangle_\mathrm{old}$, compared to (11) and (12). This agrees with our result from (6).

We have, in particular,

$$\langle n\rangle = F(\eta)N_s\langle n\rangle_1 = F(\eta)\eta\left(\frac{R_A}{r_0}\right)^2\langle n\rangle_1,$$
$$\langle p_\mathrm{T}^2\rangle = \frac{k}{k-2}\frac{\langle p_\mathrm{T}^2\rangle_1}{F(\eta)} \tag{18}$$

and the p_T^2 dispersion

$$Dp_\mathrm{T}^2 = \langle p_\mathrm{T}^2\rangle\sqrt{\frac{k-1}{k-3}}. \tag{19}$$

Equations (15) and (16) summarize our main results. The multiplicity and transverse momentum distributions for any type of collision and degree of centrality are universal functions which depend only on one parameter, $\langle n_1\rangle$ and $\langle p_\mathrm{T}^2\rangle_1$ respectively. These parameters are related to γ' and γ through (13) and (14). Because of this, our parameters γ and γ' in the weight function are different.

The additional parameter k depends on η in the way that has been pointed out before. It is related to the fluctuations in the number of strings per cluster by (1) and plays an important role in the behavior of the dependence of the transverse momentum fluctuations on the number of participants [51,52]. Notice that both distributions are obtained from the same kernel, the gamma distribution, with the same parameter k. This fact implies that they are related to each other. In particular, the suppression of high p_T production in (16) is controlled by k which also provides us the width of the multiplicity distribution at high multiplicities. Due to this, we predict that in $p+p$ collisions at LHC energies, where the string densities will be very high, the k value will be higher and in consequence both

distributions, the multiplicity and transverse momentum one, will be narrower.

The relation between both distributions can be checked directly with the existing experimental data from $p+p$ collisions. In fact, fixing the k values from fits to the multiplicity distributions, we have fitted the transverse momentum distributions, with the power law $A(1+bp_{\mathrm{T}}^2)^{-k}$ obtaining an overall agreement with experimental data at $\sqrt{s}=23, 200, 630$ and 1800 GeV. The detailed comparison is done in [53].

The values $\langle n\rangle_1$ and $\langle p_{\mathrm{T}}^2\rangle_1$ stand for the average over all particles. If we are interested in the study of a particular particle species i, we shall write $\langle n\rangle_{1i}$ and $\langle p_{\mathrm{T}}^2\rangle_{1i}$.

At $\eta\to\infty$, $k\to\infty$ and the distribution (16) becomes $\exp(-F(\eta)p_{\mathrm{T}}^2/\langle p_{\mathrm{T}}^2\rangle_{1i})$, very similar to the behavior at $\eta\to 0$, $\exp(-p_{\mathrm{T}}^2/\langle p_{\mathrm{T}}^2\rangle_{1i})$.

From (16) one can calculate

$$\frac{\mathrm{d}\ln f}{\mathrm{d}\ln p_{\mathrm{T}}}=\frac{-2F(\eta)}{\left(1+\frac{F(\eta)}{k}\frac{p_{\mathrm{T}}^2}{\langle p_{\mathrm{T}}^2\rangle_{1i}}\right)}\frac{p_{\mathrm{T}}^2}{\langle p_{\mathrm{T}}^2\rangle_{1i}}\ . \tag{20}$$

As $p_{\mathrm{T}}^2\to 0$, this reduces to

$$-2F(\eta)p_{\mathrm{T}}^2/\langle p_{\mathrm{T}}^2\rangle_{1i}\ , \tag{21}$$

while for large p_{T}, it becomes $-2k$.

We use a gamma distribution for the clusters, which is reasonable due to the above mentioned arguments. It may be possible to use other distributions which have the same properties concerning the dependence of their mean value and dispersion on the centrality. The resulting multiplicity and transverse momentum distributions in that case would be very similar to (15) and (16). Nevertheless, we have additional confidence in our assumption, since the resulting multiplicity and transverse momentum distributions have a reasonable agreement with experimental data. In fact, the negative binomial distribution is in good agreement with the multiplicity distribution for $p+p$ collisions in a broad range of energies, and it can also describe the $h+A$ and $A+A$ multiplicity distributions.

The power-like behavior $(p_{\mathrm{T}}^2)^{-k}$ found for the transverse momentum distribution, with an exponent related to some intrinsic fluctuations, is common to many apparently different systems, as sociological, biological or informatics ones [54–56]. Distributions that describe the growth of the wealth of people living in stable economical systems, the distribution of the citations of the scientific works, or other complex networks where the probability $P(m)$ of having a given node with m links is described by the free scale power law $P(m)\sim(m)^{-k}$ with k close to 3 obey the same behavior. Also, it has been shown [56, 57] that maximization of the non-extensive information Tsallis entropy leads to the distribution (16).

This universal behavior indicates the importance of the common features present in those phenomena, namely, the cluster structure and the fluctuations in the number of objects per cluster.

3 Density dependence of the mean transverse momentum and k

A more specific test of these ideas can be made in a straightforward manner from (18), (19) and (4): there is a universal relation between $\left[\sqrt{\frac{\langle p_{\mathrm{T}}^2\rangle}{\langle p_{\mathrm{T}}^2\rangle_1}}\right]_i$ and $\sqrt{\frac{1}{N_A^{2/3}}\frac{\mathrm{d}n}{\mathrm{d}y}}$,

$$\left[\sqrt{\frac{\langle p_{\mathrm{T}}^2\rangle}{\langle p_{\mathrm{T}}^2\rangle_1}}\right]_i=\left(\frac{r_0}{R_1}\frac{1}{\langle n\rangle_1}\right)\sqrt{\frac{k}{k-2}}\frac{1}{F(\eta)\sqrt{\eta}}\sqrt{\frac{1}{N_A^{2/3}}\frac{\mathrm{d}n}{\mathrm{d}y}}\ . \tag{22}$$

A similar relation was suggested in the framework of the CGC model [58], and a quantitative discussion was presented in [59]. One should notice that (22) is fairly independent of the kind of particle i (π, k, p), independent of energy (from 200 GeV to 1800 GeV), and independent of the interacting nuclei (Au+Au at RHIC, p+p at Tevatron).

From comparison with data, it can be checked that $k(\eta)$ is a function with the properties enunciated in the introduction,

$$k(\eta)=\frac{2\phi^2(\eta)}{\phi^2(\eta)-1}, \tag{23}$$

with

$$\phi(\eta)=\sqrt{F(\eta)}+F(\eta)\sqrt{\eta}. \tag{24}$$

The function $k(\eta)$ has the qualitative behavior that we expect, namely, it has a minimum $k_{\min}\simeq 3$ at $\eta_{\min}=2$ and goes to infinity as $\eta\to 0$ and $\eta\to\infty$. This means that in such limits only one kind of cluster is produced. However, the minimum value of k is reached at a slightly high value of η. There are reasons to think about a modification of (24), keeping the right limits for k at $\eta\to 0$ and $\eta\to\infty$, but introducing a shift in η. In fact, $F(\eta)\sqrt{\eta}=1-\mathrm{e}^{-\eta}$ is the average fraction of the total area occupied by clusters at density η when the area is homogeneous. Actually, in a heavy ion collisions, the surface is not homogeneous when nuclei profile functions of the Wood–Saxons type are taken into account [60]. This increases the average fraction of occupied area, resulting in a faster decrease of the exponential. Due to this, we use the function given by (23) and (24) for k but introducing the shift $\eta\to b\eta$, in such a way that the minimum value of k is reached at $\eta_{\min}=0.6$ ($b=3.3$). In Fig. 2 we present the functions before and after the change. Notice that in both cases the minimum value is $k\simeq 3$, where the variance of the p_{T}^2 distribution diverges.

The main dependence of k on the energy comes from the dependence on η. In A+A collisions, as the energy increases, the density of strings increases and k increases. However, there is an additional dependence on the energy, working on the opposite way, which up to now has not been taken into account. It is well known that even in hadron–hadron collisions at $\sqrt{s}\simeq 30$ GeV, there is enough energy to produce hard scatterings. This modifies the single exponential in the transverse momentum distribution. As far as the number of strings is very low there is no possibility of overlapping. In perturbative QCD, the study of the production of n gluons leads to a distribution whose width is controlled by

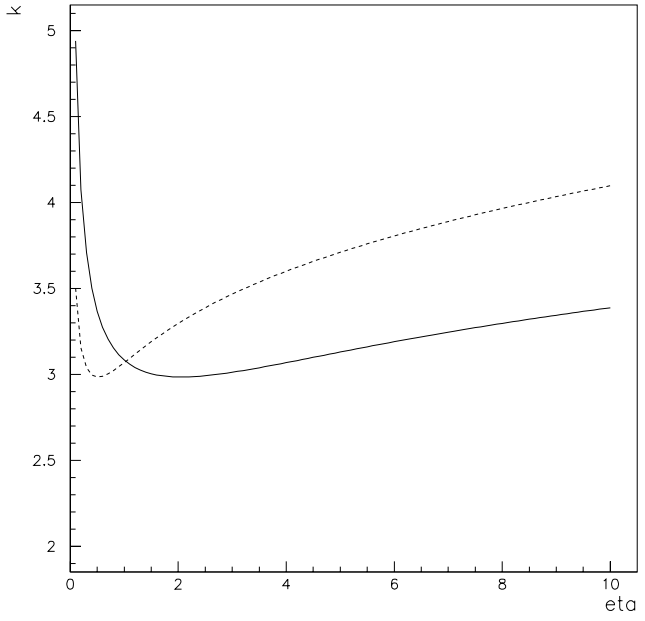

Fig. 2. Dependence of k on η, using (23) and (24) (dotted line) and changing $\eta \to 3.3\eta$ (solid line)

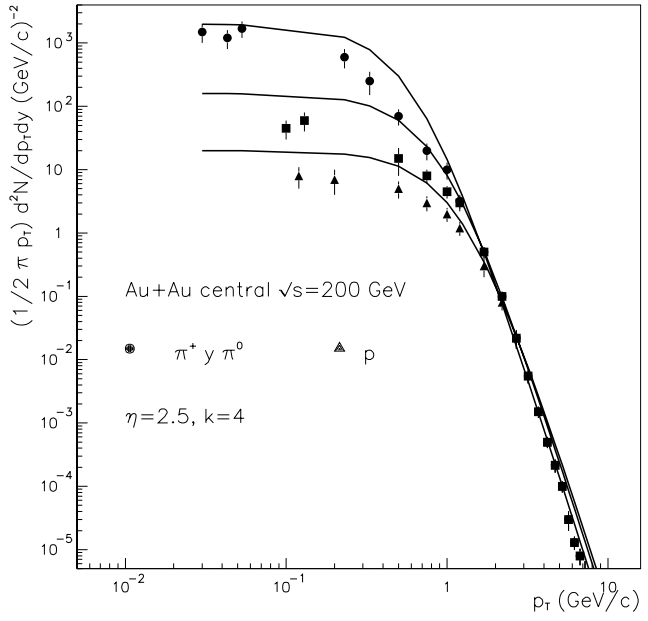

Fig. 3. Experimental PHOBOS data on low $p_{\rm T}$ distributions for pions, kaons and protons, together with our results

$k\mu$, where $\mu = 1/(1-\gamma)$, $\gamma = \sqrt{\frac{6\alpha_{\rm s}}{\pi}} - \frac{11}{8}\left(1 + \frac{2n_f}{27}\right)\frac{\alpha_{\rm s}}{\pi}$. As the energy increases, the QCD coupling constant $\alpha_{\rm s} \to 0$ and $\mu \to 1$, in such a way that asymptotically only the parameter k remains. As $k\mu$ decreases with the energy the distribution becomes broader.

To take into account this energy dependence we will use an effective k given by

$$k_{\rm eff} = k\ [a\ (\mu - 1) + 1], \tag{25}$$

with μ as defined above. We use $\alpha_{\rm s}(M_Z) = 0.122$, so $\alpha_{\rm s}(\sqrt{s} = 19.4\,{\rm GeV}) \approx 0.165$, $\alpha_{\rm s}(\sqrt{s} = 200\,{\rm GeV}) \approx 0.108$ and $\alpha_{\rm s}(\sqrt{s} = 1800\,{\rm GeV}) \approx 0.081$. The above expression satisfies $k_{\rm eff} = k$ for $s \to \infty$. The values for $\alpha_{\rm s}$ are lower that the ones used in other approaches for hadronic interactions, especially at SPS energies – at low energy, threshold effects can be not negligible. In other words to take into account these uncertainties, we have introduced the phenomenological expression (25). In this way, the dependence of k on $\alpha_{\rm s}$ is modified through the factor a.

The value of a, $a = 0.3$, was determined by the comparison of the $p_{\rm T}$ distributions for Pb + Pb collisions at SPS energies and Au + Au collisions at $\sqrt{s} = 200\,{\rm GeV}$ with the experimental data.

From now on, in order to compare with experimental data, we will use $k_{\rm eff}$ from (25). Through this equation, k – solid line in Fig. 2 – is multiplied by a factor that depends on the energy. This factor is around 1.28 at SPS energies, 1.19 at RHIC energies and 1.13 at LHC energies (5500 GeV). Note that the dependence of k on η and on the energy is model dependent, so it may suffer changes, specially at low energy where the threshold effects can be not negligible. The fact that we want to stress here is the existence of a minimum on the behavior of k versus η, related to a maximum of fluctuations, and the limits of k at low and high density, where $k \to \infty$.

4 Comparison with the experimental data

As we said before, the number of strings is computed using a Monte-Carlo code [39] based on the quark gluon string model. Knowing $N_{\rm S}$ and $r_0 = 0.25$ fm, we can compute η for each type of collision. From (23)–(25) we obtain k. Finally, the values of $\langle p_{\rm T}^2\rangle_{1p} = 0.30$, $\langle p_{\rm T}^2\rangle_{1k} = 0.14$, $\langle p_{\rm T}^2\rangle_{1\pi} = 0.06$ are normalized to reproduce the dependence of $\langle p_{\rm T}^2\rangle$ on centrality for protons, kaons and pions. Note that the different $\langle p_{\rm T}^2\rangle_1$s correspond to different γs in the original gamma distribution

With these values, we have entirely determined (16) for all types of collision energies and rapidities.

At low $p_{\rm T}$, the behavior given by (21) is clearly confirmed by PHOBOS data, namely the derivative of $\log f(p_{\rm T})$ with $\log p_{\rm T}$ vanishes as $p_{\rm T} \to 0$. As $\langle p_{\rm T}^2\rangle_{1p} > \langle p_{\rm T}^2\rangle_{1k} > \langle p_{\rm T}^2\rangle_{1\pi}$, the absolute value is larger for pions than for kaons and than for protons. At higher $p_{\rm T}$, the distributions become similar. This is shown in Fig. 3, where we present our results for Au + Au central collisions at $\sqrt{s} = 200\,{\rm GeV}$, $\eta = 2.5$, $k_{\rm eff} = 4$, together with the PHOBOS data at low $p_{\rm T}$ and PHENIX data at higher $p_{\rm T}$. Notice that in the figure there are data from two different collaborations with different normalizations. Probably, this is at the origin of the minor differences between the data and our results. (We do not fit the PHOBOS data, but just apply (16) fixing the normalization $\frac{{\rm d}n}{{\rm d}y}$ to reproduce the point at $p_{\rm T} = 2\,{\rm GeV}$.)

Now, let us discuss the interplay between low and high $p_{\rm T}$.

One defines the ratio $R_{\rm CP}(p_{\rm T})$ between central and peripheral collisions as

$$R_{\rm CP}(p_{\rm T}) = \frac{f'(p_{\rm T}, y=0)/N'_{\rm coll}}{f(p_{\rm T}, y=0)/N_{\rm coll}}, \tag{26}$$

where the distribution in the numerator corresponds to higher densities, $\eta' > \eta$. The division by $N_{\rm coll}$ essentially eliminates $N_{\rm S}$ from $\frac{{\rm d}n}{{\rm d}y}$ (this is true only at mid-rapidity) and from (16) and (6) we obtain

$$R_{\rm CP}(p_{\rm T}) = \frac{\left(\frac{k'-1}{k'}\right)}{\left(\frac{k-1}{k}\right)} \left(\frac{F(\eta')}{F(\eta)}\right)^2 \frac{\left(1+\frac{F(\eta)}{k}\frac{p_{\rm T}^2}{\langle p_{\rm T}^2\rangle_{1i}}\right)^k}{\left(1+\frac{F(\eta')}{k'}\frac{p_{\rm T}^2}{\langle p_{\rm T}^2\rangle_{1i}}\right)^{k'}} . \tag{27}$$

In the $p_{\rm T} \to 0$ limit, taking into account that $\frac{2}{3} \le \frac{k-1}{k} < 1$ and that $F(\eta') < F(\eta)$, we obtain

$$R_{\rm CP}(0) \simeq \left(\frac{F(\eta')}{F(\eta)}\right)^2 < 1 , \tag{28}$$

approximately independent of k and k'. As η'/η increases, the ratio $R_{\rm CP}$ decreases, in agreement with the experimental data.

As $p_{\rm T}$ increases, we have

$$R_{\rm CP}(p_{\rm T}) \sim \frac{1+F(\eta)p_{\rm T}^2/\langle p_{\rm T}^2\rangle_{1i}}{1+F(\eta')p_{\rm T}^2/\langle p_{\rm T}^2\rangle_{1i}} , \tag{29}$$

and $R_{\rm CP}$ increases with $p_{\rm T}$ (again, $F(\eta) > F(\eta')$).

At large $p_{\rm T}$,

$$R_{\rm CP}(p_{\rm T}) \sim \frac{F(\eta)}{F(\eta')}\frac{k'}{k} p_{\rm T}^{2\,k-k'} , \tag{30}$$

which means that if we are in the low density (low energy, low N_A) branch of the $k(\eta)$ curve, see Fig. 2, $k > k'$ and $R_{\rm CP}(p_{\rm T}) > 1$) (Cronin effect). As η'/η increases the ratio $R_{\rm CP}(p_{\rm T} \to \infty)$ increases (it must have a limit due to phase space limitations).

As we increase the energy of the nucleus–nucleus collision, the energy density increases and one has to observe the high density branch of the $k(\eta)$ curve. There, for $\eta' > \eta$, $k' > k$ and suppression on $p_{\rm T}$ occurs. The Cronin effect will disappear at high energies and/or densities.

In the forward rapidity region, the division by $N_{\rm coll}$ in (26) does not cancel $N_{\rm S}$ from $\frac{{\rm d}n}{{\rm d}y}$, since in this rapidity region $N_{\rm S}$ is proportional to N_A instead of $N_{\rm coll}$. Therefore, an additional factor $\frac{N'_A/N'_{\rm coll}}{N_A/N_{\rm coll}}$ appears now in $R_{\rm CP}(p_{\rm T})$. As $N'_{\rm coll} - N'_A$ is much larger than $N_{\rm coll} - N_A$, $R_{\rm CP}(p_{\rm T}, y=3) < R_{\rm CP}(p_{\rm T}, y=0)$, thus a further suppression occurs, in agreement with the experimental data [61,62]. In order to quantify this suppression, let us consider central and peripheral d + Au collisions at mid-rapidity and at $y = 3.2$. From the BRAHMS Collaboration data [61] at $p_{\rm T} \simeq 2$–$3\,{\rm GeV}/c$, $R_{\rm CP}(p_{\rm T}, y=3.2)/R_{\rm CP}(p_{\rm T}, y=0) \simeq 0.45/1.25 = 0.36$ for 0–20% and 60–80% degree of centrality. For these centralities, the values quoted by the collaboration are $N'_A(d) = 1.96$, $N'_{\rm coll} = 13.6$, $N_A(d) = 1.39$ and $N_{\rm coll} = 3.3$. The resulting ratio $(1.96/13.6)/(1.39/3.3) = 0.35$ is in perfect agreement with the data.

The ratio between $R_{\rm CP}(p_{\rm T})$ for two different particles, for instance p and π, becomes, at large $p_{\rm T}$,

$$\frac{R^P_{\rm CP}(p_{\rm T})}{R^\pi_{\rm CP}(p_{\rm T})} \simeq \left(\frac{\langle p_{\rm T}^2\rangle_{1P}}{\langle p_{\rm T}^2\rangle_{1\pi}}\right)^{k'-k} . \tag{31}$$

For Au + Au central and peripheral collisions at $\sqrt{s} = 200\,{\rm GeV}$, we have $k' = 4$ and $k = 3.6$ respectively. Therefore, the ratio is close to 2, in good agreement with the experimental data.

In Fig. 4, we compare our results for π^0 production in central and peripheral Au + Au and $p+p$ collisions at $\sqrt{s} = 200\,{\rm GeV}$, together with the experimental data. In Fig. 5, the nuclear modification factor for central and peripheral Au + Au collisions at mid-rapidity are shown. In Fig. 6, we show the comparison of our results for d + Au collisions at $\sqrt{s} = 200\,{\rm GeV}$ and at mid-rapidity, and in Fig. 7 we show the corresponding nuclear modification factor. In Fig. 8 we compare our results with the experimental data [63][2] for central and peripheral Pb + Pb collisions at SPS energies. We observe a reasonable agreement in all cases. Notice that the trend of the data can be understood qualitatively from our equation (16) and the ratios $R_{\rm CP}(p_{\rm T})$ or the nuclear modification factor depend on the difference $k'(\eta') - k(\eta)$ (at large $p_{\rm T}$) and on the ratio $\frac{F(\eta')}{F(\eta)}$ (at low $p_{\rm T}$), and not on the absolute values of k', k, $F(\eta')$ and $F(\eta)$, in such a way that the uncertainties in the computation of η' and η due to the values of r_0 and $N_{\rm S}$ are essentially canceled. All the explanation stems from the facts that $F(\eta') < F(\eta)$ for $\eta' > \eta$ and $k' > k$ for large densities and $k' < k$ for small densities. Finally, in Fig. 9, we show our prediction for LHC energies.

5 Back jet-like hadron correlations

One of the most interesting data from RHIC is the disappearance of back to back jet-like hadrons in Au + Au collisions, contrary to what happens in d + Au collisions. We think that the suppression of produced jets in central $A + A$ collisions is indeed due to final state interactions – jet-quenching or interactions with partons and comovers. Here, for completeness, we would like to evaluate the interaction of a quark or gluon jet with a final state formed by a cluster of strings corresponding to a given value of η. We will follow the reference [65]. In Fig. 10 we show the formation of several strings in a nucleus–nucleus collision. At high density there will be overlapping of strings in the transverse space, forming clusters. Above the percolation critical density, essentially one cluster will be formed

[2] We are aware that there is a big uncertainty concerning SPS data (see [64] for more details). Nevertheless, we use these data since they have been obtained by the same experimental collaboration as the ones we have used to fix the value of μ_1 in our model. With this value we can reproduce also multiplicities at SPS and RHIC energy. These considerations let us to have a consistent description for $p_{\rm T}$ and multiplicity distributions.

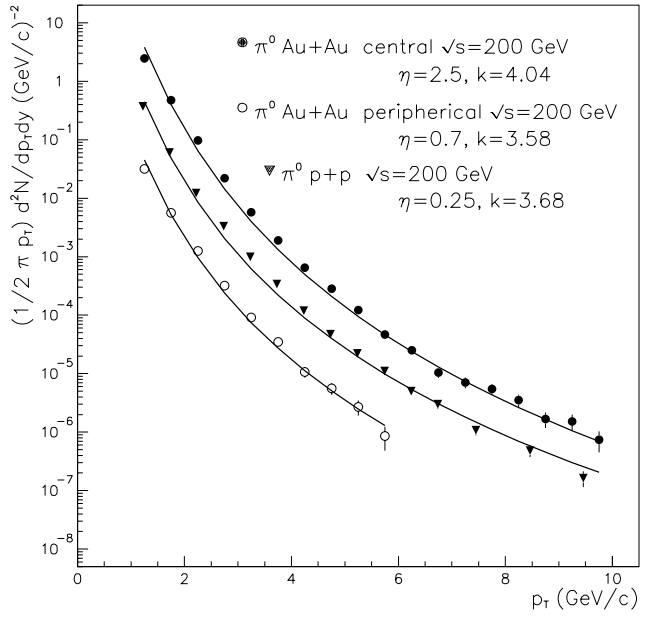

Fig. 4. Comparison between our results and experimental data from Au+Au central and peripheral collisions and p+p collisions at $\sqrt{s} = 200\,\mathrm{GeV}$

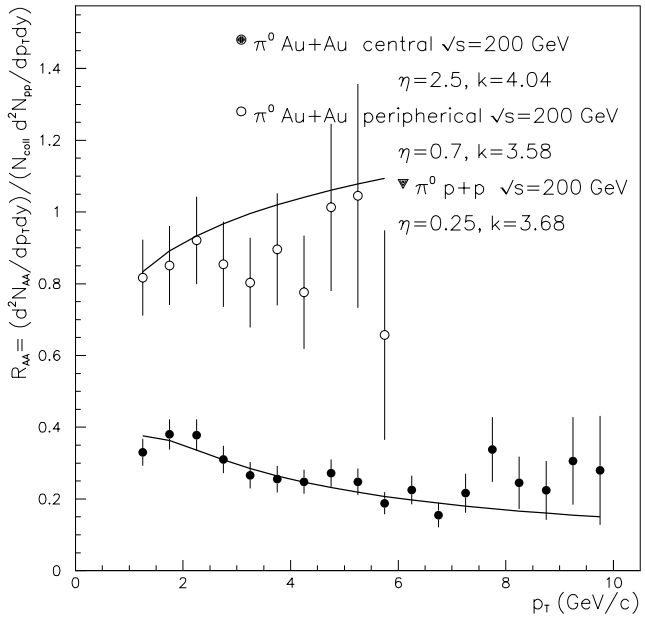

Fig. 5. Comparison between our results and experimental data on the nuclear modification factor from Au + Au central and peripheral collisions at $\sqrt{s} = 200\,\mathrm{GeV}$

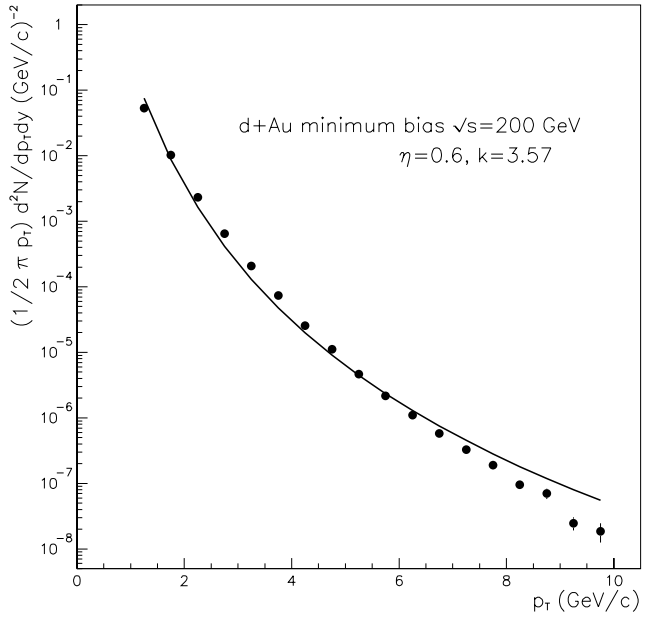

Fig. 6. Our results for d + Au minimum bias collisions at $\sqrt{s} = 200$ and mid-rapidity compared to experimental data

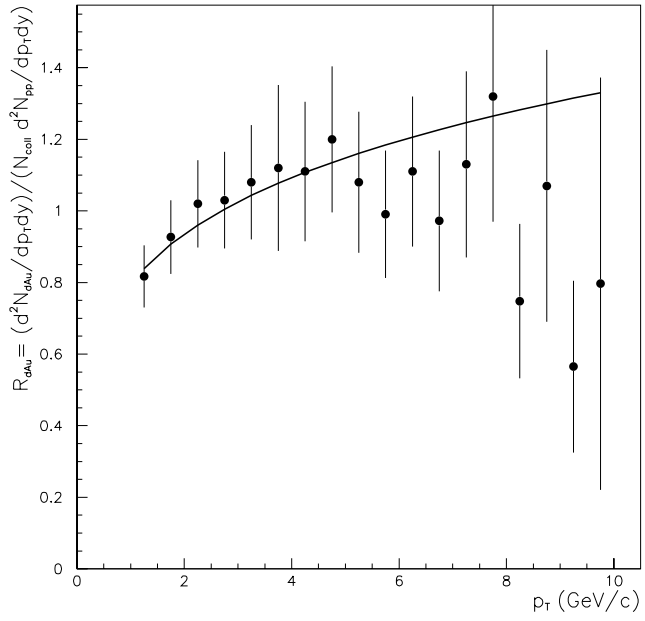

Fig. 7. Our results for d + Au minimum bias collisions at $\sqrt{s} = 200$ and mid-rapidity normalized to our results for p-p minimum bias collisions multiplied by the number of collisions, compared to the experimental data

through the whole collision area. This colorless cluster can act as a non-thermalized quark gluon plasma, where the color would no longer be confined to hadronic or flux tube dimensions but to the whole available area of the scattering.

The string-like shape of the color fields are oriented along the collision axis. Consider a hard parton–parton collision, which produces two hardly scattered partons which are moving in the transverse plane to the reaction axis and in opposite directions (Fig. 11). The interaction of these partons with QCD fields of the strings affects the parton momentum distribution, which determines the distribution of secondary particles in the jet. In particular, bremsstrahlung gluon radiation takes place in a tangential direction by the parton crossing the gluon field of each string. This gluon radiation will eventually produce low p_{T} particles. In other words, the jets are not going to disappear but are going to be degraded to lower p_{T} particles. This is at the origin of the difference found by the STAR collaboration [66] between near and away side p_{T} distributions.

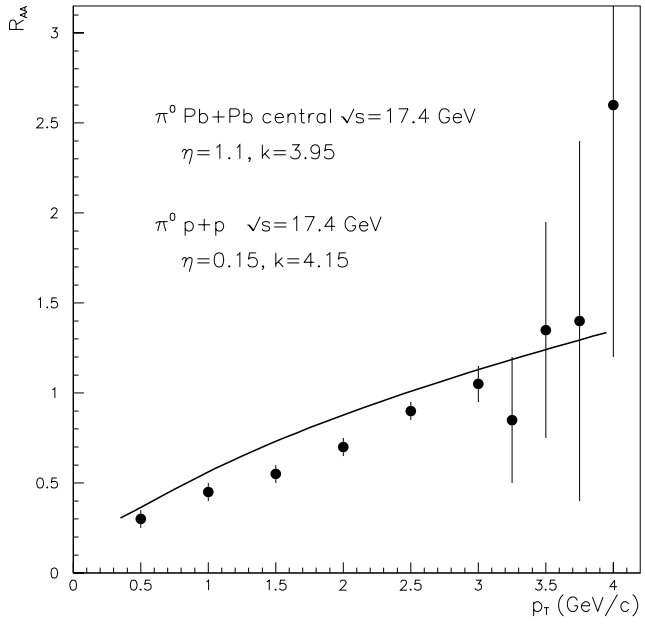

Fig. 8. Nuclear modification factor for Pb+Pb central collisions at SPS energies

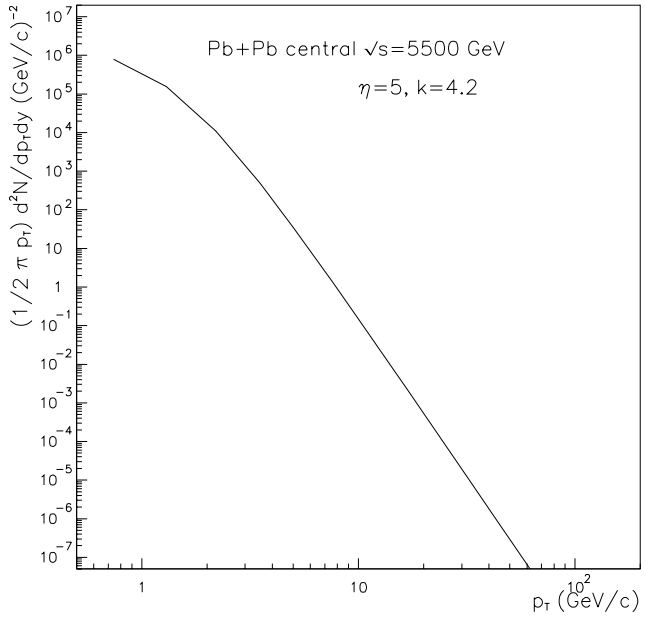

Fig. 9. Predictions for Pb + Pb central collisions at 5500 GeV

This interaction produces an asymmetry, the projection of momentum of secondary particles in the jet along the reaction axis (Fig. 10, z axis) becomes larger than in the transverse direction (x axis). Let us consider a quark q_1 passing through the flux strings transverse to the string axis. We assume a constant static uniform chromoelectric field pointed along the reaction axis. Because in the static case chromomagnetic fields vanish, the force acting on the quark q_1 can be written as

$$\vec{F} = \frac{g}{2}\lambda_1^a \vec{E^a},$$

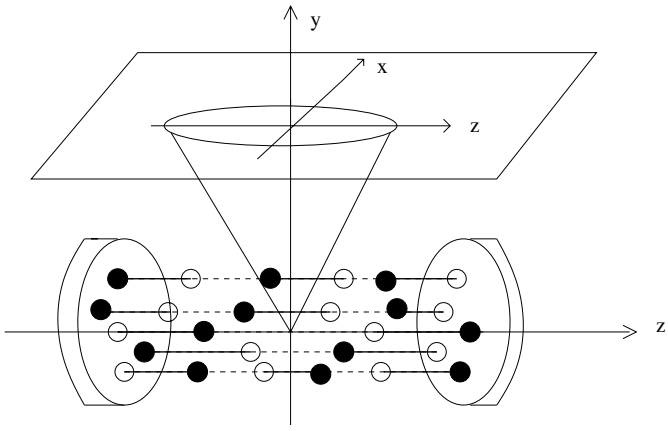

Fig. 10. Formation of strings in a nucleus–nucleus collision

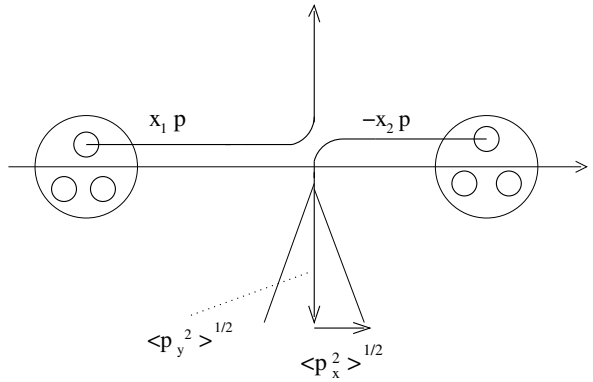

Fig. 11. Hard scattered partons that can interact with the strings

where g in the QCD coupling, $\frac{g^2}{4\pi} = \alpha_s$ and λ^a are the Gell-Mann matrices. First, we compute the change of the transverse momentum of q_1 after crossing one string. Let x and y axis be the coordinate system in the section where q_1 crosses the string, let the y axis be pointed along q_1's direction of motion and let ξ be the distance between axis y and line of q_1 movement. Then q_1 will cross the string surface in points $(\xi, y_1(\xi))$ and $(\xi, y_2(\xi))$ and the momentum change will be

$$\Delta \vec{p_1}\,(\xi) = \int \vec{F}\,(\xi,t)\mathrm{d}t = \int_{y_1(\xi)}^{y_2(\xi)} \vec{F}\,(\xi,y)\mathrm{d}y$$
$$= \int_{y_1(\xi)}^{y_2(\xi)} g\frac{\lambda_1^a}{2}\,\vec{E^a}\,(\xi,y)\mathrm{d}y\ . \qquad (32)$$

Doing the average over all ξ we obtain

$$\Delta \vec{p_1} = \frac{1}{\int_{-r_o}^{r_0}\mathrm{d}\xi}\int_{-r_0}^{r_0}\mathrm{d}\xi\int_{y_1(\xi)}^{y_2(\xi)} g\frac{\lambda_1^a}{2}\,\vec{E^a}\,\mathrm{d}y$$
$$= \frac{1}{2r_0}\int_{s_1}\mathrm{d}s\ g\frac{\lambda_1^a}{2}\,\vec{E^a}\ , \qquad (33)$$

where S_1 is the transverse string area. Applying the Gauss theorem we have

$$\Delta \vec{p_1} = \frac{\hat{\vec{z}}}{2r_0}\frac{g\lambda_1^a}{2}\int_{S_1}\vec{E}\mathrm{d}\vec{S} = \frac{\hat{\vec{z}}}{2r_0}\frac{g\lambda_1^a}{2}\int_V \mathrm{div}\,\vec{E^a}\,\mathrm{d}V$$

$$= \frac{\widehat{\vec{z}}}{2r_0}\frac{g^2}{8}\lambda_1^a\lambda_2^a, \tag{34}$$

where $\frac{g\lambda_2^a}{2}$ is the color charge of quark q_2 (string end) and $\widehat{z}$ is the unit vector in the z direction. Doing the average over the color states of q_1 and q_2, we obtain

$$\Delta p_1 = \frac{g^2}{8\pi_0}\frac{1}{2\sqrt{2}}\frac{16}{3} = \frac{4\pi\alpha_{\rm S}}{3\sqrt{2}r_0}\ . \tag{35}$$

The average number of strings crossed by the quark is

$$N = 2r_0 Lm \tag{36}$$

where L is distance traveled by the quark, $L \approx R_A$ and m is the number of strings per unit area

$$m = \frac{N_{\rm S}}{\pi R_A^2}\ . \tag{37}$$

In $A+A$ collisions at mid-rapidity, $N_{\rm S} \approx 2N_A^{4/3}$ at RHIC energies and $3N_A^{4/3}$ at LHC energies. In the forward rapidity region $N_{\rm S}$ will be $2N_A$ and $3N_A$ at RHIC and LHC energies respectively.

The mean transverse momentum of quark q_1 after it crosses N strings would be

$$\begin{aligned}\langle \Delta p_{ZN}^2\rangle &= \langle(\Delta p_{ZN-1} + \Delta p_Z)^2\rangle \\ &= \langle \Delta p_{ZN-1}^2\rangle + \langle \Delta p_Z^2\rangle + 2\langle \Delta p_{ZN-1}\Delta p_Z\rangle \end{aligned} \tag{38}$$

As Δp_{ZN-1} and Δp_Z may be pointed in any direction along the string independently, the last term vanishes and therefore

$$\langle \Delta p\rangle_{\rm tot} \simeq \sqrt{N}\Delta p_1\ . \tag{39}$$

For $\alpha_{\rm S} \simeq 0.3$ and $r_0 = 0.2$–0.25, we obtain from (35) $\Delta p_1 \simeq 0.9$–$0.75\,{\rm GeV}/c$. For central Au + Au collisions at mid-rapidity we obtain $\sqrt{N} \simeq 5.5$–7. Then $\langle \Delta p\rangle_{\rm tot} \simeq 4.9$–$5.2\,{\rm GeV}/c$, which is comparable with the $p_{\rm T}$ triggered; therefore the back to back jet-like correlations disappears. On the contrary, for central $d+$Au collisions, $\sqrt{N} \simeq 0.75$–0.85 and $\langle \Delta p\rangle_{\rm tot} \simeq 0.67$–$0.64\,{\rm GeV}/c$, which is much smaller than the $p_{\rm T}$ of the triggered jet, $p_{\rm T} > 4\,{\rm GeV}/c$, and the back to back jet-like correlation survives. An intermediate situation is Au + Au central collisions at forward rapidity, where $\sqrt{N} \simeq 2.5$–3.2 and $\langle \Delta p\rangle_{\rm tot} \simeq 2.2$–$2.4\,{\rm GeV}/c$. In this case, the back to back jet structure is only partially destroyed. In the case of peripheral collisions, the suppression would be stronger when the jet is perpendicular to reaction plane (the plane spanned by the beam axis and the impact parameter, $b \neq 0$) than when the jet is in the reaction plane, in agreement with the experimental data. Notice that before we deduced stronger suppression at forward than at mid-rapidities for the nuclear modification factor but we predict less suppression of the jet. In the first case, the origin of the further suppression is the normalization of the clustering in the initial state and in the second case, the lower interaction of the quark jet with the final state is due to the smaller string densities present at forward rapidities.

Finally, let us mention that, in the framework of the CGC, it has been also found stronger depletion of the back to back correlations in $p+A$ and $A+A$ collisions than in the case of $p+p$ collisions [67].

6 Conclusions

We have obtained a universal transverse momentum distribution that allows us to describe the low $p_{\rm T}$ shape of the different particle species and the suppression of the high $p_{\rm T}$ yield compared to the scaling with the number of collisions, $N_{\rm coll}$, expected on the basis of the factorization theorem of QCD.

The shape of this distribution is determined essentially by two functions, $F(\eta)$ and $k(\eta)$, which depend on the density of the color sources η. The first one stems from the dynamics of the color clusters, and it is at the origin of the suppression of the multiplicity. It also controls the transverse momentum distribution of the produced particles due to the fragmentation of the cluster. The second one, $k(\eta)$, is related to the fluctuations in the number of strings per cluster. At low density, k decreases with the density and, on the contrary, at high density it increases with the density.

The fact that for $p+$Au and $d+$Au central collisions the densities are not far from the minimum of k explains the Cronin effect. It will disappear at higher energy or higher densities because of the increase of k. In the forward rapidity region, the number of color sources scales with the number of participant nucleons, N_A, while in the central rapidity region it scales with the number of collisions $N_{\rm coll} \propto N_A^{4/3}$. Therefore, comparing the $p_{\rm T}$ yield scaled by the number of collisions, in the forward rapidity region there will be a suppression due to the additional factor $1/N_A^{1/3}$.

The multiplicity distributions are related to the transverse momentum ones through the cluster size distribution, whose width is controlled by k. At high mean multiplicities the relative dispersion of the multiplicity distribution is given by $1/k$, decreasing as the energy increases.

The disappearance of the back to back jet-like hadron correlations in Au + Au collisions is a final state interaction due to the interaction of the quark jet with the cluster of strings formed in the initial state. This cluster is less dense in the forward rapidity region, so we predict a smaller suppression of the correlation in this case.

We can conclude that the clustering of color sources provides us with a framework suitable to describe the main features of the transverse momentum and multiplicity distributions at RHIC and SPS energies. This, together with the successful explanation of the dependence of the fluctuations of transverse momentum on the number of participants and the dependence on the multiplicity of the strength of the two-body and three-body correlations, favors this approach.

We are aware of the limitations of our framework, coming mainly from the lack of a direct derivation from QCD. Also, we do not included any hard component in the single string. Therefore, at fixed energy and above some $p_{{\rm T}m}$ our

picture will fail. However, as the energy and the density grow, there are more overlapping strings which extend the validity of the description to a higher $p_{\mathrm{T}m}$. Finally, asymptotically, our picture is valid for all transverse momentum, recovering a single exponential, $\exp(-F(\eta)p_{\mathrm{T}}^2/\langle p_{\mathrm{T}}^2\rangle_i)$.

Our approach has similarities with the CGC. In both approaches there is clustering – of gluons in the CGC and of color sources in our approach. In both approaches, the initial state interactions – gluon saturation in the CGC or clustering of color sources in the percolation approach – produce a suppression of the p_{T} distributions. In CGC the gluon field is renormalized as the color charge increases. In our approach, we have redefined our main variables for the cluster as the color density increases. The suppression of the high p_{T} yield and the saturation of the multiplicity per participant at high density are related to each other and they are a consequence of the saturation of gluons at the scale given by the saturation momentum Q_{S} in the CGC [68]. The clustering of strings produces also the suppression of p_{T} and the independence of the multiplicity per participant on N_A. We obtain, as in the CGC, larger suppression of the p_{T} yield at forward rapidity, and also we predict that the Cronin effect would disappear at higher energies. Both approaches obtain a scaling for the transverse momentum distributions. We make an extension of the soft spectra to the region of hard p_{T} by means of clustering of strings. The CGC does an extension of the hard region to the soft one by means of clustering of gluons; therefore in a broad range of p_{T} both approaches should coincide.

In QCD, the distribution for n gluons is approximately given, in the modified leading log approximation, by the generalized gamma function [69]

$$\frac{\Gamma_n}{\Gamma} \sim \frac{1}{\langle n\rangle}\left(\frac{n}{\langle n\rangle}\right)^{k\mu-1}\exp\left(-D\frac{n}{\langle n\rangle}\right)^{\mu}, \qquad (40)$$

whose width becomes broader as the energy increases. According to our considerations we expect a narrower width of this distribution above a certain density. It would be welcome to have a proof of that.

Let us remark that another possibility of testing our approach is to study the behavior of the forward–backward correlations which are proportional to the fluctuations in the number of independent clusters. At moderate density, we expect a rise of these correlations as it is observed at $p+p$ and $h+A$ collisions. On the contrary, at high density, these long range correlations should disappear as a consequence of the formation of a large cluster of strings [70]. A similar behavior is expected in the CGC.

Finally, let us comment that our approach provide us with an initial state which can affect the final state interactions, as it was shown above when we studied the disappearance of back jet-like correlations.

This means that other phenomena as jet-quenching or interaction with comovers are not necessarily contradictory to our approach. We only claim that at low and intermediate p_{T}, $p_{\mathrm{T}} \leq 4$–$5\,\mathrm{GeV}/c$, the percolation of color sources is able to give a simple and reasonable description of the data.

Acknowledgements. We thank M.A. Braun, N. Armesto, F. del Moral, C.A. Salgado for discussions. This work has been done under contracts FPA2002-01161 of CICyT of Spain, POCTI/36291/FIS/2000 of Portugal, Feder funds from EU and PGIDIT03PXIC20612PN from Galicia.

References

1. S.S. Adler et al., PHENIX Collaboration, Phys. Rev. C **69**, 034910 (2004); Phys. Rev. Lett. **91**, 072301 (2003)
2. J. Adams et al., STAR Collaboration, Phys. Rev. Lett. **91**, 172302 (2003)
3. B.B. Back et al., PHOBOS Collaboration, Phys. Lett. B **578**, 297 (2004)
4. J.C. Collins, D.E. Soper, G. Sterman, Nucl. Phys. B **308**, 831 (1998)
5. I. Arsene et al., BRAHMS Collaboration, Phys. Rev. Lett. **91**, 072305 (2003)
6. S.S. Adler et al., PHENIX Collaboration, Phys. Rev. Lett. **91**, 0722303 (2003)
7. J. Adams et al., STAR Collaboration, Phys. Rev. Lett. **91**, 072304 (2003)
8. J. Adams et al., STAR Collaboration, Phys. Rev. Lett. **92**, 112301 (2004)
9. B.B. Back et al., PHOBOS Collaboration, nucl-ex/0401006
10. C. Adler et al., STAR Collaboration, Phys. Rev. Lett. **90**, 082302 (2003)
11. M. Chiu et al., PHENIX Collaboration, Nucl. Phys. A **715**, 761 (2003)
12. S.S. Adler et al., PHENIX Collaboration, nucl-ex/0310005
13. J. Adams et al., STAR Collaboration, nucl-ex/0308033
14. L.V. Gribov, E.M. Levin, M.G. Ryskin, Phys. Rep. **100**, 1 (1983); A.H. Muller, J. Qiu, Nucl. Phys. B **268**, 427 (1986); J.P. Blaizot, A.H. Mueller, Nucl. Phys. B **289**, 847 (1987)
15. L.D. McLerran, R. Venugopalan, Phys. Rev. D **49**, 2233 (1994); D **49**, 3352 (1994); D **50**, 2225 (1994)
16. E. Iancu, A. Leonidov, L.D. McLerran, Nucl. Phys. A **692**, 583 (2001); E.G. Ferreiro, E. Iancu, A. Leonidov, L.D. Mclerran, Nucl. Phys. A **710**, 5414 (1997); A.L. Ayala, M.B. Gay Ducati, E.M. Levin, Nucl. Phys. B **493**, 305 (1997); J. Jalilian-Marian, A. Kovner, H. Weigert, Phys. Rev. D **59**, 014015 (1999)
17. N. Armesto, M.A. Braun, E.G. Ferreiro, C. Pajares, Phys. Rev. Lett. **77**, 3736 (1996); M. Nardi, H. Satz, Phys. Lett. B **442**, 14 (1998); E.G. Ferreiro, hep-ph/0409264
18. A. Capella, A. Kaidalov, J. Tran Thanh Van, Heavy Ion Physics **9**, 169 (1999); E.G. Ferreiro, hep-ph/0409287
19. V.N. Gribov, The theory of complex angular momenta (Cambridge Univ. Press, 216 2003)
20. M.A. Braun, C. Pajares, Phys. Rev. Lett. **85**, 4864 (2001); Eur. Phys. J. C **16**, 349 (2000)
21. M.A. Braun F. del Moral, C. Pajares, Phys. Rev. C **65**, 024907 (2002)
22. M.A. Braun, C. Pajares, hep-ph/0405203, Phys. Lett B to appear
23. V.N. Gribov, Nucl. Phys. B **139**, 1 (1978); J. Greensite, Ch.B. Thorn, JHEP **0202**, 014 (2002); G. 't Hooft, Nucl. Phys. Proc. Suppl. **121**, 333 (2003); Yu.L. Dokshitzer, D.E. Kharzeev, hep-ph/0404216
24. M. Gyulassy, X.N. Wang, Nucl. Phys B **420**, 580 (1994); M. Gyulassy, I. Vitev, X.N. Wang, Phys. Rev. Lett. **86**, 2537

(2001); C.A. Salgado, U.A. Wiedemann, Phys. Rev. Lett. **89**, 092303 (2002); R. Baier, Y.L. Dokshitzer, A.A. Mueller, S. Peigne, D. Schiff, Nucl. Phys. **483**, 291 (1997)
25. A. Capella, E.G. Ferreiro, A. Kaidalov, D. Sousa, hep-ph/0403081; nucl-th/0405067
26. B.Z. Kopeliovich, J. Nemchik, A. Schaefer, A. V. Tarasov, Phys. Rev. Lett. **88**, 232303 (2002); D. Kharzeev, Y.V. Kovchegov, K. Tuchin, Phys. Rev. D **68**, 094013 (2003); V.A. Abramovsky, N.V. Prikhod'ko, Eur. Phys. J. C **35**, 359 (2004); E. Cattaruzza, D. Treleani, Phys. Rev. D **69**, 094006 (2004); A. Accardi, M. Gyulassy, Phys. Lett. B **586**, 244 (2004); M.A. Braun, E.G. Ferreiro, C. Pajares, D. Treleani, Nucl. Phys. A **723**, 249 (2003); E. Iancu, K. Itakura, D.N. Triantafyllopoulos, Nucl. Phys. A **742**, 182 (2004); J.P. Blaizot, F. Gelis, R. Venugopalan, Nucl. Phys. A **743**, 13 (2004); J. Jalilian-Marian, nucl-th/0402080
27. J.L. Albacete, N. Armesto, A. Kovner, C. Salgado, U. Wiedemann, Phys. Rev. Lett. **92**, 082001 (2004)
28. H.G. Dosch, Yu.A. Simonov, Phys. Lett. B **205**, 339 (1988)
29. Yu.A. Simorov, J. Tjon, Ann. Phys. **300**, 54 (2002)
30. A. Di Giacomo, H.G. Dosch, V.I. Shevchenko, Yu.M. Simorov, Phys. Rep. **372**, 319 (2002)
31. A. Kaidalov, K.A. Ter-Martirosyan, Phys. Lett. B **117**, 247 (1982)
32. A. Capella, U.P. Sukhatma, C.I. Tan, J. Tran Thanh Van, Phys. Rep. **236**, 225 (1994); A. Capella et al., Z. f. Physik C **33**, 541 (1987)
33. E.L. Bratkovskaya et al., Phys. Rev. C **69**, 054907 (2004); H. Weber, E.L. Bratkovskaya, W. Cassing, H. Strocker, Phys. Rev. C **67**, 014904 (2003)
34. Ben-Hao Sa, Au Tai, Phys. Rev. C **62**, 044905 (2000)
35. S.A. Bass et al., Prog. Part. Nucl. Phys. **42**, 255 (1998)
36. L.V. Bravina et al., Phys. Rev. C **60**, 024904 (1999)
37. V.K. Magas, L.P. Csernai, D.D. Strottman, Nucl. Phys. A **712**, 167 (2002)
38. F.W. Bopp, J. Ranft, R. Engel, S. Roesler, Acta Phys. Pol. B **35**, 303 (2004)
39. N.S. Amelin, N. Armesto, C. Pajares, D. Sousa, Eur. Phys. J. C **22**, 149 (2001)
40. J. Schwinger, Phys. Rev. D **82**, 664 (1951)
41. B. Andersson, G. Gustafson, G. Ingerlman, T. Sjõstrand, Phys. Rep. **97**, 31 (1983); B. Andersson, The Lund model (Cambridge Univ. Press 1998)
42. M.A. Braun, F. del Moral, C. Pajares, Eur. Phys. J. C **21**, 557 (2001); F. del Moral, C. Pajares, Nucl. Phys. (Proc. Suppl.) **92**, 342 (2001)
43. M.A. Braun, F. del Moral, C. Pajares, Phys. Lett. B **551**, 291 (2003)
44. A. Capella, C. Pajares, A.V. Ramallo, Nucl. Phys. B **241**, 75 (1984)
45. J. Dias de Deus, R. Ugoccioni, Phys. Lett. B **494**, 53 (2000)
46. M. Kutchera, K. Werner, Z. Phys. C **45**, 91 (1989); Phys. Lett. B **220**, 243 (1989)
47. G. Jona-Lasinio, Nuovo Cimento B **26**, 99 (1975)
48. J. Dias de Deus, C. Pajares, C.A. Salgado, Phys. Lett. B **408**, 417 (1997); B **407**, 335 (1997); B **409**, 474 (1997); J. Dias de Deus, C. Pajares, Phys. Lett. B **442**, 395 (1998)
49. S. Hegyi, Phys. Lett. B **441**, 321 (1997); Phys. Lett. B **466**, 380 (1999)
50. M.A. Braun, C. Pajares, Phys. Lett. B **444**, 435 (1998)
51. E.G. Ferreiro, F. del Moral, C. Pajares, Phys. Rev. C **69**, 034901 (2004)
52. J. Dias de Deus, A. Rodrigues, hep-ph/0308011
53. J. Dias de Deus, E.G. Ferreiro, C. Pajares, R. Ugoccioni, hep-ph/0405116
54. R. Gallagher, T. Appenzeller, Science **284**, 79 (1999); C. Koh, G. Laurent, Science **284**, 96 (1999)
55. R. Albert, H. Jeong, A.L. Barabasi, Nature **400**, 130 (1999); R. Albert, A.L. Barabasi, Rev. Mod. Phys. **74**, 47 (2002); Science **286**, 509 (1999)
56. G. Wilk, Z. Wlodarczyk, Acta Phys. Pol. B **35**, 2141 (2004); Phys. Rev. Lett. **84**, 2770 (2000)
57. C. Tsallis, J. Statist. Phys. **52**, 479 (1988)
58. L. McLerran, J. Schaffner-Bielich, Phys. Lett. B **514**, 29 (2001); J. Schaffner Bielich, D. Kharzeev, L. McLerran, R. Venugopalan, Nucl. Phys. A **705**, 494 (2002)
59. J. Dias de Deus, E.G. Ferreiro, C. Pajares, R. Ugoccioni, Phys. Lett. B **581**, 156 (2004)
60. A. Rodrigues, R. Ugoccioni, J. Dias de Deus, Phys. Lett. B **458**, 402 (1999); J. Dias de Deus, R. Ugoccioni, A. Rodriges, Eur. Phys. J. C **16**, 537 (2000)
61. R. Debbe, BRAHMS Collaboration, J. Phys. G **30**, S759 (2004); I. Arsene et al., nucl-ex/0403005
62. A. Ogawa, STAR Collaboration, nucl-ex/0408004
63. M.M. Aggarwal et al., WA98 Collaboration, Phys. Rev. Lett. **85**, 3595 (2000)
64. D. d'Enterria, Phys. Lett. B **596**, 32 (2004)
65. M.Yu. Kopysov, Yu.E. Pokrovsky, hep-ph/9705326
66. F. Wang, STAR Collaboration, J. Phys. G **30**, S1299 (2004)
67. D. Kharzeev, E. Levin, L. McLerran, hep-ph/0403271
68. D. Kharzeev, M. Nardi, Phys. Lett. B **507**, 121 (2001); D. Kharzeev, E. Levin, Phys. Lett. B **523**, 79 (2001)
69. Yu.L. Dokshitzer, Phys. Lett. B **305**, 295 (1993); V.A. Khoze, W. Ochs, Int. J. Mod. Phys. A **12**,
70. N. Amelin, N. Armesto, M. Braun, E.G. Ferreiro, C. Pajares, Phys. Rev. Lett. **73**, 2813 (1994); M.A. Braun, R.S. Kolevatov, C. Pajares, V.V. Vechernin, Eur. Phys. J. C **32**, 535 (2004)